

# Oxygen Doped Hierarchically Porous Carbon for Electrochemical Supercapacitor

Ning Zhao<sup>1,2,3</sup>, Libo Deng<sup>2</sup>, Dawei Luo<sup>3</sup>, Shuting He<sup>1</sup> and Peixin Zhang<sup>1,2,\*</sup>

<sup>1</sup> School of Materials & Mineral Resources, Xi'an University of Architecture and Technology, Xi'an, Shanxi 710055, China

<sup>2</sup> College of Chemistry and Environmental Engineering, Shenzhen University, Shenzhen 518060, China

<sup>3</sup> School of chemistry and biological application, Shenzhen Polytechnic, Shenzhen 518055, China

\*E-mail: [pxzhang@szu.edu.cn](mailto:pxzhang@szu.edu.cn)

Received: 23 July 2018 / Accepted: 1 September 2018 / Published: 1 October 2018

---

Carbon is the promising candidate served as electrode material for electrochemical capacitors, due to its merits in good electrical conductivity, high surface area and relatively low cost. Pore size distribution is an important factor for carbon based electrode materials. Herein, oxygen-doped hierarchical porous carbon (OPC) was synthesized by a two-step low cost carbonization and KOH activation process of pomelo mesocarp. Oxygen functional groups were introduced to the structure and served as hydrophilizing agent, which highly contributes to the permeation of electrolyte into the inner pores of the OPC material. The as prepared OPC material delivers a superhigh specific surface area at 2378.1 m<sup>2</sup>/g and a large pore volume at 1.13 cm<sup>3</sup>/g. Electrochemical performances of the OPC electrode show a high capacitance of 292 F/g at 0.5 A/g and excellent cycling stability with capacitance retention of 96.41 % over 1000<sup>th</sup> cycle at 1 A/g.

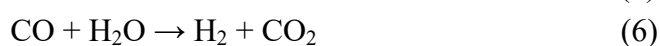
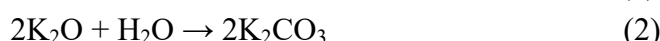
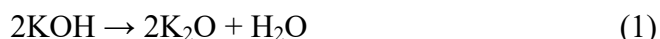
---

**Keywords:** Supercapacitor; Waste biomass; Activated carbon; 3D porous.

## 1. INTRODUCTION

The exploitation of novel materials application for next generation energy storage devices by utilizing environmentally friendly strategies is urgent driven by sustainable development of human society.[1] Supercapacitors was recognized as an promising energy storage device and applied in many fields, such as memory backup sources, portable electronics, hybrid electric vehicles, regenerative and renewable energy systems, due to its high power density, long cycle life and low maintenance cost. Based on their different charge-storage mechanisms, supercapacitors commonly include electrical double layer capacitors (EDLCs) and pseudocapacitors. Pseudocapacitors store electrical energy

through redox reactions, electrosorption and intercalation processes. Transition metal oxides and conductive polymers are usually applied as pseudocapacitors electrode materials. However, the cycle stability and low electrical conductivity leave much to be desired of the practical applications of pseudocapacitors. The energy storage of electric double layer capacitors (EDLCs) usually originates from the adsorption of electrolyte ions at electrode/electrolyte interfaces. Namely, surface charges are accumulated on the electrode surfaces and opposite charge ions are arranged in the electrolyte side. Correspondingly, high specific surface area and pores adjusted to the ionic size are favorable to enhance the electrochemical performance of EDLC. The existence of micropores in the carbon materials can significantly increase the specific surface area. However, the electrolyte ions show difficulty diffusing into or through the deep micropores of activated carbon, resulting in the increase of charging time. It was recognized that well developed network between mesopores and micropores is beneficial for the diffusion of electrolyte ions. As a result, 3D hierarchical and interconnected porous structure has attracted great research interests in recent years. Carbon materials is the widely used electrode materials for supercapacitors due to their excellent electrical conductivity, good physical and chemical stability as well as morphology controllable feature.[2] In consideration of environmentally benign nature, the use of waste biomass sources for the preparation of carbon materials has become the focus of materials scientists. It was identified to be a sustainable and environmental friendly method to converse the waste biomass into valuable carbonaceous material. In this respect, multifarious waste biomass sources such as walnut shells,[3] coconut shell,[4] pistachio nutshells,[5] sunflower seeds shells,[6] watermelon rind,[7] banana peels[8] and so on were investigated as electrode materials for electrochemical capacitors. Activating agents such as  $K_2CO_3$ ,[9]  $ZnCl_2$  [10] and particularly  $KOH$ [11] have been utilized. For example, the activation mechanism of the  $KOH$  can be shown in the following equations: [12]



Pomelo mesocarp, a widely distributed biomass material, has been widely utilized to synthesis carbon based materials for energy applications in recent years.[13] In this work, oxygen-doped porous carbonaceous (OPC) material was successfully prepared by using pomelo mesocarp as raw material through a two-step  $KOH$  activation procedure.  $KOH$  acts as pore forming and activating reagent to improve the specific surface area of OPC material.[14] The intermediate product  $K_2CO_3$  and  $K_2O$  generated in the carbon particle left behind macropores after subsequent washing processes (see eq. (1)-(2)). Micropores, however, were produced owing to the deodorize of the K metal vapor above the boiling point of  $762\text{ }^\circ\text{C}$  and diffused into carbon matrix (eq. (3)-(4)).[12] Therefore, the  $KOH$  activating temperature was fixed at  $800\text{ }^\circ\text{C}$  to acquire all the micro-, meso- and macro-pores in the typical activating process. The obtained OPC material possesses a 3D porous structure with a high specific surface area of  $2378.1\text{ m}^2/\text{g}$  and displays an outstanding electrochemical performance with a

high specific capacitance up to 292 F/g at 0.5 A/g as well as excellent cycling stability, due to the increased hydrophilicity, defects and porosity of the carbon material.

## 2. EXPERIMENT

### 2.1. Materials preparation

Pomelo mesocarp material was acquired from the fruit market (the pomelo grown in the Guangdong region of China). Acetylene black and Polytetrafluoroethylene were purchased from Shenzhen Kejing Star Technology. Co., LTD..

Pomelo mesocarp was dried under 80 °C for 12h before use. In a typical synthesis, dried pomelo mesocarp was pre-carbonized under 300 °C in air atmosphere for 1h to reserve and generate oxygen containing groups. Then, KOH and the pre-carbonized pomelo mesocarp were mixed with a mass ratio of 1:3. The mixture was subsequently heated under 800 °C for 1h in N<sub>2</sub> atmosphere. After cooling, OPC material can be obtained by washing with diluted HCl and distilled water for several times, and then dried at 110 °C overnight.

### 2.2. Characterization

The structure of the prepared OPC material was measured by X-ray power diffraction (XRD) on Rigaku D/Max-2550V diffractometer using Cu<sub>Kα</sub> radiation. The morphology of the samples was measured by scanning electron microscope (SEM JEOL S-4800) and transmission electron microscope (TEM 30 JEOL JEM-2100F). The specific surface area of products was examined by Brunauer-Emmett-Teller (BET) method (V-Sorb 2800P, Gold APP, China). The pore size distributions were calculated from desorption branches of the isotherms through Barrett-Joyner-Halenda (BJH) method. FTIR spectra of products were recorded on a Nicolet 7000-C, Thermal Scientific Co., USA.

### 2.3. Electrochemical measurements

The working electrodes were prepared by mixing the synthesized OPC material, acetylene black and polytetrafluoroethylene (PTFE) binder with a weight ratio of 80:10:10 in water to form slurry. The obtained slurry was then pressed onto a nickel foam (1\*1 cm<sup>2</sup>) current collector. The as coated nickel foam was dried at 60 °C for several hours before pressed under a pressure of 10 MPa. Each electrode contained about 1 mg active material. The working electrode was dipped in 6 M KOH aqueous electrolyte. Regarding the three electrodes test, a platinum plate and a Hg/HgO electrode was used as counter electrode and reference electrode, respectively. Cyclic voltammeters (CV) were carried out on a electrochemical workstation (CHI660E, Shanghai, China) with a voltage range between -1.0-0 V (vs Hg/HgO) at different scan rates from 10 to 200 mV/s. Electrochemical impedance spectroscopy (EIS) measurements were conducted in the frequency range from 0.01 to 100 kHz with an amplitude of 5 mV at an open-circuit potential. For galvanostatic charging-discharging measurement, the current densities were varied from 0.5 to 10 A/g within the same potential range as in cyclic voltammetry measurements on a LAND CT2001A cell measurement system.

The specific capacitance of electrodes was evaluated from the discharging curves at different current densities according to the following equation:[15]

$$C = I \times t / (\Delta V \times m) \quad (7)$$

Where  $C(\text{F/g})$  is the specific capacitance of the electrode,  $I(\text{A})$  is the constant discharging current,  $t(\text{s})$  is the discharging time,  $\Delta V(\text{V})$  is the voltage change during discharging excluding the IR drop, and  $m(\text{g})$  is the mass of active materials on one electrode.

### 3. RESULTS AND DISCUSSION

SEM and TEM images clearly evidence the successful formation of the 3D porous structure. As can be seen in Fig. 1(a), the as obtained material has an interconnected 3D porous network. The high magnification SEM image shows that the pore size was in the range from 500 nm to several micrometers (Fig. 1(b)). These pores are created by the cross-linking between the carbon walls. Further amplify the material by TEM, both micropores and mesopores can be found on the carbon walls (Fig. 1(c)). Macropores are favor to shorten the electrolyte ion diffusion pathway, while the existence of mesopores can provide more area to deliver higher specific capacitance. High-resolution TEM image (Fig. 1(d)) reveals a partial graphitic feature of the obtained OPC material, which is consistent with the following results of XRD and Raman spectrum.

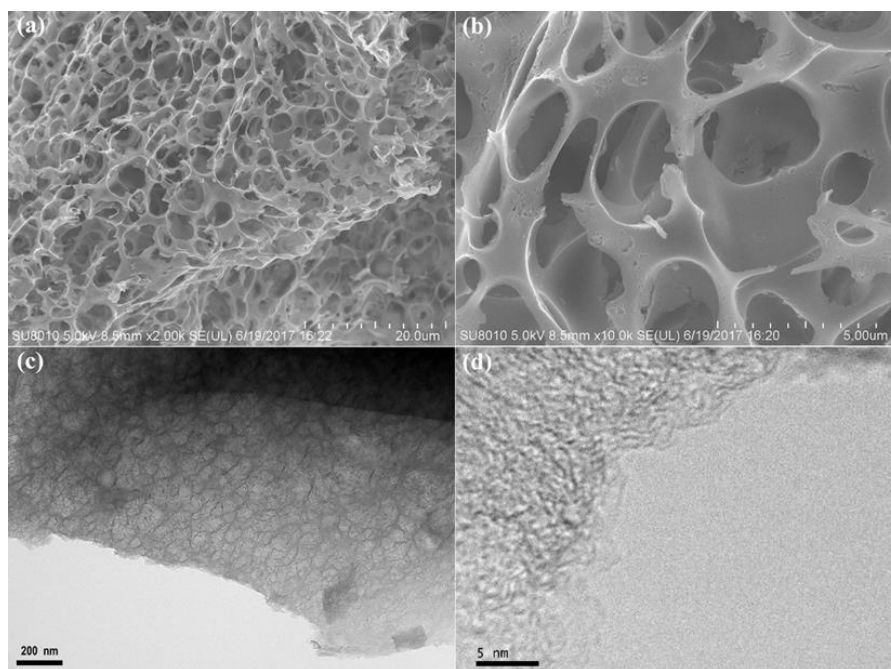


**Figure 1.** (a) low-magnification; and (b) high-magnification SEM images; (c) low-resolution; and (d) high-resolution TEM images for the prepared OPC material.

The powder XRD pattern and Raman spectra was widely employed to characterize the structure and defects of carbon based materials. The XRD pattern of OPC (Fig. 2(a)) material exhibits two broad peaks at  $2\theta$  around  $23^\circ$  and  $44^\circ$ , which can be ascribed to the (002) and (100) reflections, respectively.[16] The broad diffraction peaks indicate the amorphous and disordered state of the

prepared OPC material.[17] Two prominent D and G band shown in Raman spectrum (Fig. 2(b)) also suggest the highly disordered graphitic structures for the produced OPC material.[1] As we know, the G band at around  $1585\text{ cm}^{-1}$  corresponds to ideal graphitic lattice vibrational mode with  $E_{2g}$  symmetry. The D band, around  $1340\text{ cm}^{-1}$ , is homologous with the defect or disorder in carbon material. The intensity ratio of the D band to G band ( $R = I_D/I_G$ ) is evaluated to be 1.15, indicating low degree of graphitic crystalline structure.[18]

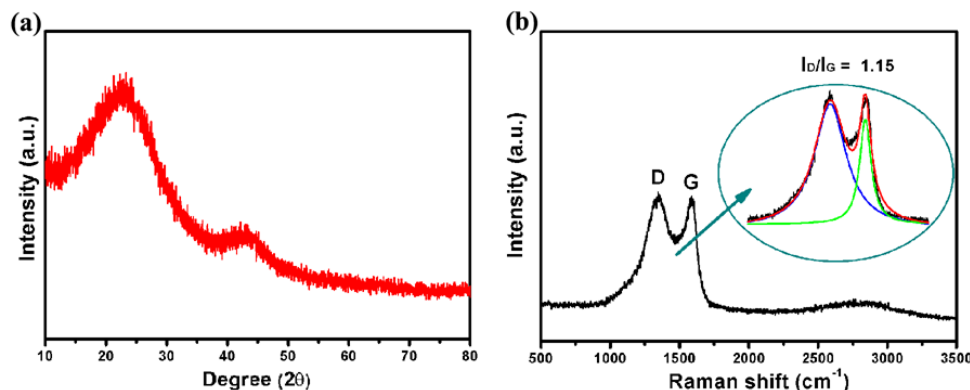


**Figure 2.** (a) XRD pattern; and (b) Raman spectrum for the prepared OPC material.

Fourier transform infrared spectroscopy spectrum (FTIR, Fig. 3(a)) was performed to characterize the functional groups in the OPC sample. Strong peaks at  $3435$ ,  $1629$ ,  $1400$ , and  $1151\text{ cm}^{-1}$  were recorded due to the vibration of O-H, C=C configurable vibration from the aromatics, C-OH bending vibrations from carbonyl groups and stretching vibrations from C-O epoxy groups, respectively. This result indicates the existence of oxygen containing groups in the prepared OPC material. To further investigate the porosity feature of the OPC material, the specific area and the pore size distribution were examined by nitrogen adsorption-desorption isotherm analysis at 77K in Fig. 3(b)-(d). The specific surface area is evaluated to be  $2378.1\text{ m}^2\text{ g}^{-1}$  for OPC sample. Nitrogen adsorption/desorption isotherms loops (Fig. 3 (b)) presented that the OPC sample mainly located in the micropores region. Moreover, the hysteresis loop in the relative pressure  $P/P_0$  range of 0.4 to 0.8 shows that a fraction of mesopores exists in the 3D porous structure, which is confirmed by the TEM images. Both of the pore area and pore volume distributions plots illustrate that the OPC sample has an average pore sizes about 2.3 nm in the range of mesopores, calculated by the BJH method (Fig. 3(c)-(d)). Massive amount of micropores exists in the OPC material. The high surface area of OPC can be ascribed to the hierarchical 3D porous structure, which composed large number of macropores as the skeleton and mesopores and micropores in the carbon wall of every macropores. The large specific surface area can provide high availability of electrode materials to electrolyte, and the appropriate pore size facilitate better diffusion and accession of electrolyte ions through pore channels during the charge storage process. It was revealed that both micropores and mesopores are beneficial for the charge storage, indicating that electrolyte ions are able to diffuse through a well-developed network between mesopores and micropores. From this point, OPC material with larger specific surface area and 3D porous structure with a wide pore size distribution could be a wonderful electrode material. To study in

detail, the electrochemical performances of the prepared OPC material were examined in the following section.

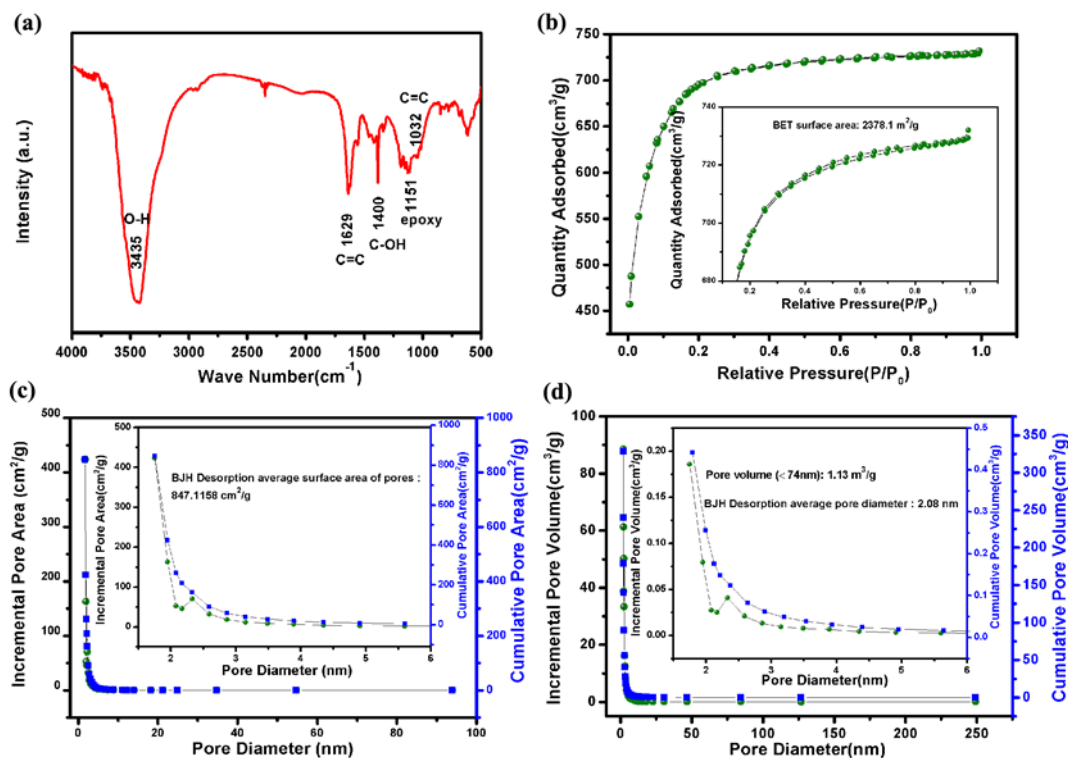


**Figure 3.** (a) FTIR spectrum; (b) Nitrogen adsorption-desorption isotherm loops; BJH desorption of (c) pore area; and (d) pore volume distribution curves for the OPC material.

The cyclic voltammograms (CV) measurements of OPC material were recorded at various scan rates of 10, 20, 50, 100 and 200  $\text{mV s}^{-1}$  in the potential range of -1.0-0 V using a three electrodes configuration (Fig. 4(a)). We can find that all the CV curves of the obtained OPC material are typical quasi-rectangular shape without any redox peaks, indicating a pure electrical double-layer capacitive behavior.[19] This shows that the oxygen functional groups have small contribution to the specific capacity of the OPC electrode. To investigate in detail, galvanostatic charge/discharge measurements were carried out, as depicted in Fig. 4(b). All the discharge curves are linear and symmetrical to their charge curves, suggesting double-layer capacitance behavior.[20] Based on galvanostatic discharge curves, the specific capacitances can be calculated. As demonstrated in Fig. 4(c), the specific capacitance values of OPC electrode are calculated to be 296, 223, 181, 150, and 132  $\text{F g}^{-1}$  at current densities of 0.5, 1, 2, 5 and 10  $\text{A g}^{-1}$ , respectively.

It is generally known that the cycling performance of electrode materials is an important factor for supercapacitor. Hence, the cycling stability of the capacitance performance of OPC electrode was evaluated by measuring the cycle performance at a current density of 1  $\text{A g}^{-1}$  (Fig. 4(d)). The OPC electrode material shows a specific capacitance of 223  $\text{F g}^{-1}$  at the first cycle and maintain as high as 215  $\text{F g}^{-1}$  after 1000 cycles, indicating a capacitance retention of 96.41 %. These results reveal that the high specific capacitance and excellent cycling stability are achieved in OPC material for supercapacitors.

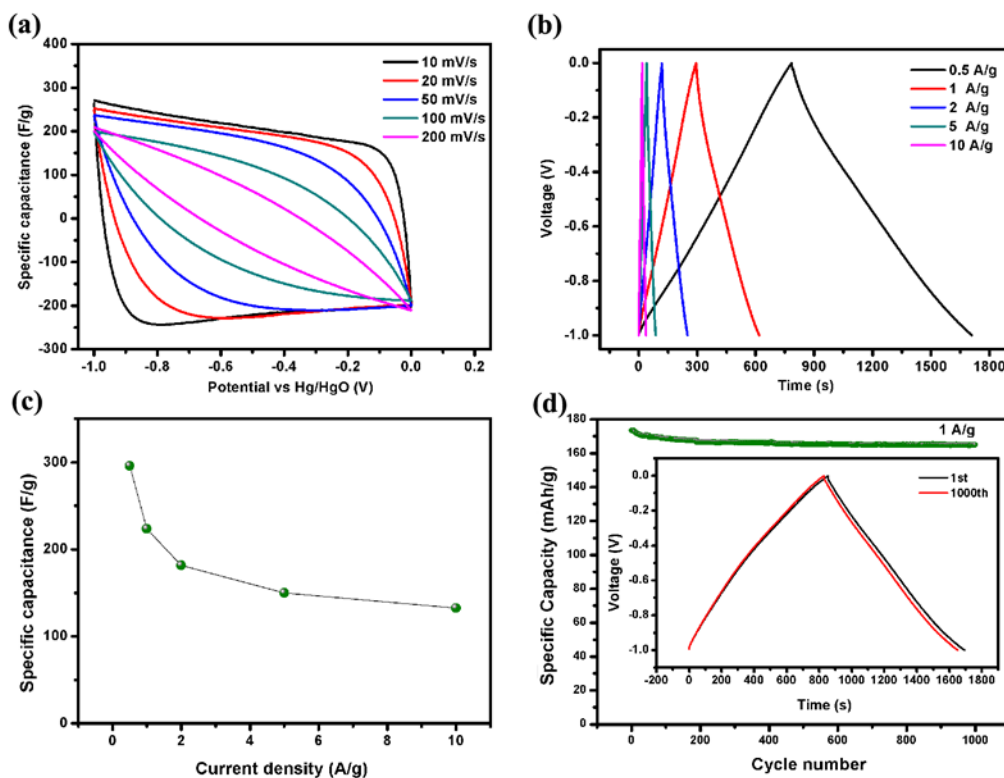


**Figure 4.** (a) CV curves of three electrode configuration at various scan rates. (b) Galvanostatic charge-discharge curves at different current densities. (c) Dependence of specific capacitance on the current density. (d) Cycling performance of specific capacitance at current density of  $1 \text{ A g}^{-1}$  (inset is galvanostatic charge-discharge curves before and after 1000th cycle) for the OPC electrode.

To further investigate the ionic conductivity of the OPC electrode, AC impedance measurement was performed between 0.01 and 100 kHz, as shown in Fig. 5(a). The EIS spectrum consists of a semi-circle in the high frequency region and a straight line almost parallel to the longitudinal axis in the low frequency region, indicating a capacitive behavior. Fig. 5(b) shows the Bode phase angle-frequency plot, in which the low frequency region of the phase shift is nearly  $-90^\circ$ , revealing a nearly identical double-layer charge storage behavior.[21, 22] This result has a good agreement with the CV and galvanostatic charge-discharge curves of the OPC electrode. The intercept on the horizontal axis in the high frequency region mainly represents the ohmic resistance of the electrolyte plus the electrode material and the contact resistance at the interface of OPC material/Ni foam current collector (short as  $R_s$ ), which is only  $1.005 \Omega$ , suggesting a very good electronic conductivity of the OPC material. The semi-circle relates to the interfacial charge transfer resistance ( $R_{ct}$ ) between the electrode and the electrolyte.[22] The  $R_{ct}$  value was evaluated to be  $1.484 \Omega$ , implying the rapid charge transfer between the electrolyte and electrode interface. Time constant  $\tau$  represents the minimum time needed to discharge all the energy from the device with an efficiency of more than 50%.[23] To calculate the time constant, the frequency response of the OPC electrode has been modeled with a single series resistor-capacitor circuit.[24] As can be seen in Fig. 5(c), the characteristic frequency  $f_0$ , which corresponds to the peak of imaginary capacitance, is about 1.47 Hz. Therefore, the time constant is calculated to be 0.68 s in view of  $\tau = 1/f_0$ , suggesting a very fast frequency

response. This means the maximum accessibility of the electrolyte ions from the outer surface layer to the inside of OPC material is only 0.68 s. This rapid frequency response could be ascribed to the existence of the 3D porous structure, which favors of accelerating the ion transport speed by giving access to the electrolyte inside the deeper pores. The interconnected macro- and meso-pores channels can act as an electrolyte reservoir and their surface-micropores adsorb electrolyte ions without needing to pull the ions deep inside the micropore, which will increase the surface area available for adsorption of electrolyte ions.[25] Besides, the oxygen hydrophilic groups on each macropores, mesopores and micropores are very benefit for the diffusing of the electrolyte ions. As a result, the as obtained OPC material would be an excellent electrode material for electrochemical capacitors.

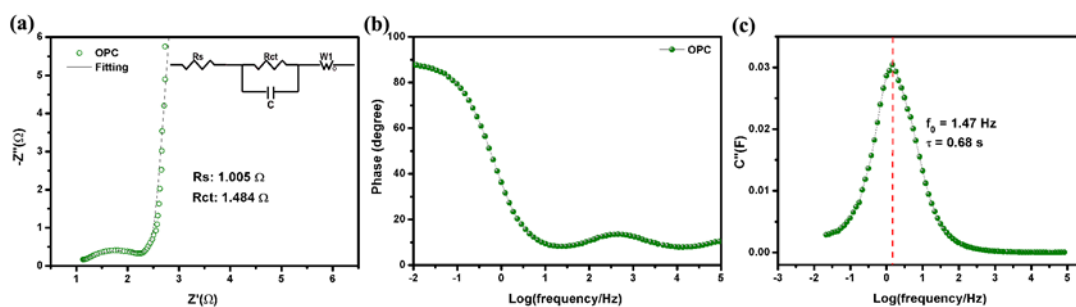


**Figure 5.** (a) Nyquist plots and fitting results of OPC sample. (b) Plot of the phase angle versus frequency; (c) plot of the real part of the capacitance against frequency.

#### 4. CONCLUSION

In summary, oxygen doped porous carbon (OPC) material with highly specific surface area was prepared by a two-step low cost method using waste biomass pomelo mesocarp as carbon source. The as synthesized OPC material possesses a 3D porous structure with a high specific surface area of  $2378.1 \text{ m}^2 \text{ g}^{-1}$  and displays a remarkable electrochemical performance with a substantially high specific capacitance up to  $292 \text{ F g}^{-1}$  at  $0.5 \text{ A/g}$ . It also exhibits an excellent cyclic stability after 1000 cycles with capacitance retention of as high as 96.41 % under  $1 \text{ A/g}$ , suggesting the promising application in electrochemical capacitor. From this work, we open up a view that the existence of the 3D porous structure and the oxygen functional groups are propitious to the charge storage.

#### ACKNOWLEDGMENTS

We gratefully acknowledge the financial support by Youth Innovative Talent Project of Guangdong Province College (2017).

#### References

1. J. Y. Liu, H. P. Li, H. S. Zhang, Q. Liu, R. M. Li, B. Li, J. Wang, *J. Solid State Chem.*, 257 (2018) 64.
2. A. G. Pandolfo, A. F. Hollenkamp, *J. Power Sources*, 157 (2006) 11.
3. W. Wang, J. Q. Qi, Y. W. Sui, Y. Z. He, Q. K. Meng, F. X. Wei, Y. X. Jin, *J. Nanosci. Nanotechno.*, 18 (2018) 5600.
4. C. M. Ashraf, K. M. Anilkumar, B. Jinisha, M. Manoj, V. S. Pradeep, S. Jayalekshmi, *J.*

- Electrochem. Soc.*, 165 (2018) A900.
5. J. D. Xu, Q. M. Gao, Y. L. Zhang, Y. L. Tan, W. Q. Tian, L. H. Zhu, L. Jiang, *Sci. Rep.-Uk*, 4 (2014) 5545.
  6. H. Y. Zhang, H. J. Niu, Y. M. Wang, C. Wang, X. D. Bai, S. Wang, W. Wang, *Pigm. Resin Technol.*, 44 (2015) 7.
  7. R. J. Mo, Y. Zhao, M. Wu, H. M. Xiao, S. Kuga, Y. Huang, J. P. Li, S. Y. Fu, *Rsc Adv.*, 6 (2016) 59333.
  8. Y. K. Lv, L. H. Gan, M. X. Liu, W. Xiong, Z. J. Xu, D. Z. Zhu, D. S. Wright, *J. Power Sources*, 209 (2012) 152.
  9. D. Adinata, W. M. A. W. Daud, M. K. Aroua, *Bioresource Technol.*, 98 (2007) 145.
  10. B. B. Chang, Y. L. Wang, K. M. Pei, S. M. Yang, X. P. Dong, *Rsc Adv.*, 4 (2014) 40546.
  11. A. Elmouwahidi, Z. Zapata-Benabithé, F. Carrasco-Marin, C. Moreno-Castilla, *Bioresource Technol.*, 111 (2012) 185.
  12. J. Matos, M. Labady, A. Albornoz, J. Laine, J. L. Brito, *J. Mol. Catal. a-Chem.*, 228 (2005) 189.
  13. S. D. Zhang, J. Liu, P. P. Huang, H. Wang, C. Y. Cao, W. G. Song, *Sci. Bull.*, 62 (2017) 841.
  14. H. J. Liu, Y. Zhang, Q. Q. Ke, K. H. Ho, Y. T. Hu, J. Wang, *J. Mater. Chem. A*, 1 (2013) 12962.
  15. Z. Wang, Y. T. Tan, Y. L. Yang, X. N. Zhao, Y. Liu, L. Y. Niu, B. Tichnell, L. B. Kong, L. Kang, Z. Liu, F. Ran, *J. Power Sources*, 378 (2018) 499.
  16. Y. H. Dong, W. X. Wang, H. Y. Quan, Z. N. Huang, D. Z. Chen, L. Guo, *Chemelectrochem*, 3 (2016) 814.
  17. Y. W. Zhu, S. Murali, M. D. Stoller, K. J. Ganesh, W. W. Cai, P. J. Ferreira, A. Pirkle, R. M. Wallace, K. A. Cychosz, M. Thommes, D. Su, E. A. Stach, R. S. Ruoff, *Science*, 332 (2011) 1537.
  18. W. Gao, L. B. Alemany, L. J. Ci, P. M. Ajayan, *Nat. Chem.*, 1 (2009) 403.
  19. W. Xing, C. C. Huang, S. P. Zhuo, X. Yuan, G. Q. Wang, D. Hulicova-Jurcakova, Z. F. Yan, G. Q. Lu, *Carbon*, 47 (2009) 1715.
  20. Q. G. Shao, J. Tang, Y. X. Lin, J. Li, F. X. Qin, J. S. Yuan, L. C. Qin, *J. Power Sources*, 278 (2015) 751.
  21. A. Bello, F. Barzegar, D. Momodu, J. Dangbegnon, F. Taghizadeh, N. Manyala, *Electrochim. Acta*, 151 (2015) 386.
  22. J. P. Wang, Y. L. Xu, J. B. Zhu, P. G. Ren, *J. Power Sources*, 208 (2012) 138.
  23. M. Sevilla, A. B. Fuertes, *Acs Nano*, 8 (2014) 5069.
  24. P. L. Taberna, P. Simon, J. F. Fauvarque, *J. Electrochem. Soc.*, 150 (2003) A292.
  25. L. Chang, D. J. Stacchiola, Y. H. Hu, *ACS Appl. Mater. Inter.*, 9 (2017) 24655.